Copyright Warning & Restrictions

The copyright law of the United States (Title 17, United States Code) governs the making of photocopies or other reproductions of copyrighted material.

Under certain conditions specified in the law, libraries and archives are authorized to furnish a photocopy or other reproduction. One of these specified conditions is that the photocopy or reproduction is not to be "used for any purpose other than private study, scholarship, or research." If a, user makes a request for, or later uses, a photocopy or reproduction for purposes in excess of "fair use" that user may be liable for copyright infringement,

This institution reserves the right to refuse to accept a copying order if, in its judgment, fulfillment of the order would involve violation of copyright law.

Please Note: The author retains the copyright while the New Jersey Institute of Technology reserves the right to distribute this thesis or dissertation

Printing note: If you do not wish to print this page, then select "Pages from: first page # to: last page #" on the print dialog screen

NJIT
New Jersey's Science & Technology University

The Van Houten library has removed some of the personal information and all signatures from the approval page and biographical sketches of theses and dissertations in order to protect the identity of NJIT graduates and faculty.

ABSTRACT

EFFECT OF TEMPERATURE ON THE FRACTURE BEHAVIOR OF LEAD-FREE SOLDER JOINTS

by
Patrick Thompson

The objective of the present study is to examine the effect of temperature on the fracture behavior of Cu-SAC305-Cu joints. To this end, double cantilever beam (DCB) specimens, consisting of a thin layer of Sn96.5Ag3.0Cu0.5 (SAC305) solder sandwiched between two copper bars, fabricated under standard surface mount (SMT) processing conditions are fractured under various temperatures with a MTS machine equipped with an environment chamber. The load-displacement behavior corresponding to crack initiation and the subsequent toughening before ultimate failure and the displacements near crack tip are recorded and used to calculate the fracture energy release rates. The fracture surfaces and the crack path analyses are conducted with a scanning electron microscope to understand the effect of temperature on the mechanism of fracture. These results provide new information to manufacturers of microelectronics packages, which could be used to further improve package reliability.

EFFECT OF TEMPERATURE ON THE FRACTURE BEHAVIOR OF LEAD-FREE SOLDER JOINTS

by
Patrick Thompson

A Thesis
Submitted to the Faculty of
New Jersey Institute of Technology
in Partial Fulfillment of the Requirements for the Degree of
Master of Science in Mechanical Engineering

Department of Mechanical and Industrial Engineering

May 2016

Blank Page

APPROVAL PAGE

EFFECT OF TEMPERATURE ON THE FRACTURE BEHAVIOR OF LEAD-FREE SOLDER JOINTS

Patrick Thompson

Dr. Siva P. Nadimpalli, Thesis Advisor — Date
Assistant Professor of Mechanical and Industrial Engineering, NJIT

Dr. I. Joga Rao, Committee Member — Date
Professor & Chair of Mechanical and Industrial Engineering, NJIT

Dr. Anthony D. Rosato, Committee Member — Date
Professor of Mechanical and Industrial Engineering, NJIT

Dr. Shawn A. Chester, Committee Member — Date
Assistant Professor of Mechanical and Industrial Engineering, NJIT

BIOGRAPHICAL SKETCH

Author: Patrick Thompson

Degree: Master of Science

Date: May 2016

Undergraduate and Graduate Education:

- Master of Science in Mechanical Engineering,
  New Jersey Institute of Technology, Newark, NJ, 2016
- Bachelor of Science in Mechanical Engineering,
  New Jersey Institute of Technology, Newark, NJ, 2014

Major: Mechanical Engineering

ACKNOWLEDGMENT

I would like to thank Dr. Siva Nadimpalli for serving as my thesis advisor and mentor. I would also like to thank the members of my committee: Dr. Shawn A. Chester, Dr. I. Joga Rao and Dr. Anthony D. Rosato, for their service and support.

I am grateful to the American Society for Engineering Education for selecting me as a Science, Mathematics and Research for Transformation scholar and funding my Master of Science degree.

I am thankful for the support of the department's laboratory technical staff, including: Joseph Glaz, Greg Policastro and Nick Muscara. I would also like to thank Richard Johnson, Raj Tripuraneni and Shuolun Wang for their contributions to this project.

TABLE OF CONTENTS

Chapter **Page**

1 INTRODUCTION……....................... ……………….……………………………. 1

1.1 Background Information........................ ………………………………….. 1

2 EXPERIMENTAL PROCEDURES ……………….……………………………. 5

2.1 Specimen Preparation.……………………………………………………….. 5

2.2 Fracture Tests…………….…………………………………….……………. 9

3 J-INTEGRAL AND FINITE ELEMENT MODELING…………………….………… 11

3.1 The J-Integral…………………..…………………………….………………… 11

3.2 Finite Element Calculation of J_c……………………………………………….. 12

4 RESULTS AND DISCUSSIONS …………….. 15

4.1 Crack Initiation and J_c…………………………….…………….……………. 15

4.2 Crack Path Analysis……………..……………………………………….…….. 17

5 CONCLUSIONS…………….... ………………………………………………..….... 21

5.1 Summary of Findings ……………….……………….……………..…............ 21

5.2 Future Work ………….....………………………………….…....................... 21

REFERENCES……………...………………………………………..….............. 22

LIST OF TABLES

Table **Page**

2.1 Number of Specimens Tested at each Temperature…....………..………………. 10

3.1 Mechanical Properties used in the Finite Element Analysis…………………….. 14

LIST OF FIGURES

Figure **Page**

1.1 Schematic of Ball Grid Array package…………………………………………..…. 1

2.1 Schematic of a DCB specimen…………………………………………………... 5

2.2 Image of sample preparation set-up………………….…………………………... 7

2.3 Time-temperature profile a DCB specimen during its fabrication…………………. 8

2.4 Image of the DCB specimen before and after machining……………….…..….... 8

2.5 Image of (a) experimental set-up. (b) DCB in chamber…………………………. 10

3.1 (a) Schematic of the change in potential energy of a nonlinearly elastic material. The shaded region can be estimated from J-Integral Calculations. (b) Crack enclosed by contours……….…………………………………………………….. 12

3.2 Finite element mesh of DCB with loads and boundary conditions……………… 14

4.1 Load-displacement response of DCB sample……………………………………. 16

4.2 Fracture energy release rates…………………………………………….…...….… 17

4.3 Fracture surface of DCB tested at (a) 22 º. (b) 100 ºC.……..…………………….... 19

4.4 SEM Images of samples tested at (a) 22 ºC. (b) 100 ºC…………………………. 20

CHAPTER 1

INTRODUCTION

1.1. Background Information

Microelectronic packages experience thermal and mechanical loading conditions throughout the course of their assembly, testing and service life. Research on microelectronic package reliability has primarily been focused on solder joint failure due to thermal fatigue. However, the mechanical strength of solder joints is also an important performance characteristic in many devices. This is especially true in higher density array packages, larger printed circuit boards and electronic devices for aerospace and automotive applications, where mechanical loads could be a significant cause of failure during service and assembly [1,2]. Figure 1.1 contains a schematic of one such high density array package. Most existing experimental methods [2-6] to evaluate the strength of solder joints under mechanical loads are qualitative and do not provide fundamental mechanical properties which can be used to predict the strength of joints in other configurations or under different loads. Therefore, tests such as the ball shear [1,2], ball pull [3], board level bending [4] and board level drop tests [5,6] are useful for quality control, but do not yield any data that can be used for failure prediction.

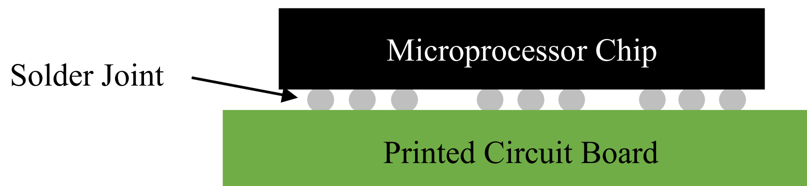

Figure 1.1 Schematic of Ball Grid Array package.

Tan et al. [7] have proposed a force-based failure criterion by measuring the strength of individual 500 μm Sn-Pb solder balls subjected to different combinations of normal and shear loads and created a force-based failure envelope. Using this force-based criterion, they were able to predict the failure of solder joints in a board level bending test. Though these results illustrated the roles of loads normal and parallel to the plane of the solder joint, they only proved useful for the particular type of joint for which the force envelope was developed. The critical strain energy release rate, G_{Ic}, as a function of the mode ratio loading [8-10], a fracture based criterion, has been used widely to predict failure in adhesive joints. G_{Ic} is an indication of the ability of a material or joint to resist crack propagation. Nadimpalli et al. [11] have used this fracture based criterion to predict the fracture loads of lead-free solder joints under mixed-mode, i.e., a combination of tensile and shear, loading conditions. Huang [12] used the critical strain energy release rate as a criterion to determine the effects of dwell time, cooling rate, and aging on the fracture toughness of SAC387 solder. However, the focus of the above studies [1-12] was on the fracture behavior of joints under a constant temperature.

It is known that temperature changes can alter the mechanical behavior, including fracture, of various materials [13]. For example, Kanel et al. [14] have studied the dynamic fracture properties of aluminum and magnesium at various temperatures ranging from room temperature to near melting temperature and showed that the material's spall strength dropped steeply as the temperature approached the melting temperature. Similarly, Zhu et al. [15] found that the tensile and impact strength of dissimilar welds in rotor steels decreased significantly with temperature. Likewise, the temperature will alter the fracture behavior of solder joints in microelectronic packages. Hence, packaging

designs without the knowledge of temperature effects on fracture will lead to poor reliability. In spite of the importance of temperature on the failure of solder joints during service, none of the above studies on solder [1-12] investigated the effect of temperature on the fracture behavior of solder joints. In one of the only studies, Logsdon et al. [16] measured the effect of temperature on the fracture properties of a lead-based solder by performing experiments at -55 °C, 24 °C and 125 °C. However, this study employed the compact tension sample, testing the solder as a bulk material which will be of limited use in prediction of joint failure; hence, the solder should be tested in a joint configuration, instead of a bulk material. Studying the solder as a bulk material prohibited this group from measuring the effect of Cu_6Sn_5 intermetallic microstructure on the joint failure.

Although G_{Ic} is a better fracture parameter to characterize the failure of solder joints compared to critical force based parameters, there are some limitations. The G_{Ic} is a valid parameter for characterizing the fracture behavior of nominally brittle materials, i.e., materials such as ceramics or ductile materials under high triaxial constraints, for which the plastically deforming region near the crack tip is negligible. However, solder, being a low strength material, will have a large plastic zone near the crack tip [13,17]. In such cases, the J integral characterizes this fracture behavior. Nadimpalli et al. [18] have used this method in their study of mixed-mode loading on solder joints.

The objective of the present study was to examine the effect of temperature on the fracture behavior of Cu-SAC305-Cu joints. To this end, double cantilever beam (DCB) specimens, prepared by sandwiching a thin layer (430 μm) of solder between two Cu bars, were subjected to mode-I fracture. Fracture energy, or J_c, was measured under various temperatures. The fracture surfaces of the samples were then analyzed to

understand the mechanism of failure and how temperature influenced this failure mechanism.

CHAPTER 2

EXPERIMENTAL PROCEDURES

2.1 Specimen Preparation

DCB specimens consisted of two copper bars (C110 Alloy, 114.3 × 12.7 × 12.7 mm) joined with a continuous layer of 430 μm thick Sn3.0Ag0.5Cu (SAC305) solder as shown in Figure 2.1. The Cu bars were cut to the required dimensions and the bonding surfaces were polished for 5 minutes using an orbital sander with an ultra-fine silicon carbide/nylon mesh abrasive pad. In order to avoid edge rounding, twelve bars were placed adjacent to one another and sanded simultaneously. Nadimpalli et al. [11] have shown that this process will produce a repeatable surface roughness. Upon completion of the polishing process, the Cu bars were rinsed with water, dried with a cloth and then rinsed with acetone. Rinsing with acetone ensured that any organic contaminants, which might have prohibited the bonding process, were removed.

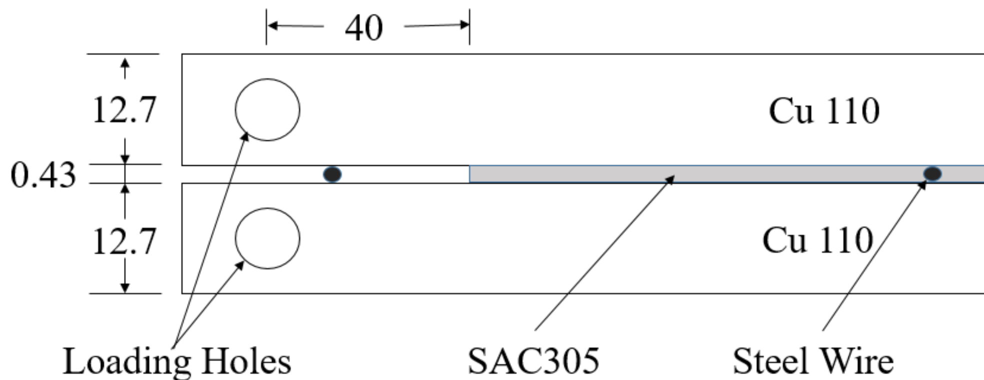

Figure 2.1 Schematic of a DCB specimen (all dimensions in mm).

Kapton tape and round steel wires were used to mask the solder joint areas and maintain the required 430 μm gap between Cu bars, respectively. The masked copper bars were placed on a hot plate, which was covered with aluminium foil and maintained at 317 ˚C, with the bonding surface vertical. Thermocouples were fixed to the top of the bars with Kapton tape to continuously monitor the temperature during the bonding process. When the temperature reached approximately 220˚C, a flux-cored SAC305 0.75mm solder wire was touched to the polished surfaces, until the bars were coated with a thin layer of solder. The solder wire was kept warm on the hot plate to facilitate a quick melting process. The bars were then clamped together against the 430 μm steel wires to maintain the required solder thickness.

The joining process, from the time of first solder application through the 100s dwell period, took approximately 120s. During this bonding process the Cu dissolves into solder layer and the Sn diffuses into Cu to form Cu_6Sn_5 intermetallic at the interface [11]; the microstructure at this interface, i.e., intermetallic morphology, is very sensitive to the time spent above the melting temperature of solder and 120s is close to the microelectronic manufacturing standards. The desired 120s above liquidus resulted in a peak temperature of approximately 240˚C which is another factor that controls the joint microstructure. The specimens were then placed transversely on supports in a wind tunnel and cooled at a rate of 1.1-1.3 ˚C/s, which is typical of the microelectronics industry. Great care was taken in designing a wind tunnel which could, consistently, provide a cooling rate of approximately 1.2 ˚C/s; repeatability in the cooling process was critical as it influences the solder microstructure. An image of the wind tunnel and a characteristic time-temperature profile can be seen in Figures 2.2 and 2.3. Preparing these specimens according to the specifications

of a previous study [11] ensured that the intermetallics and bulk solder were similar to those typical of commercial SAC305 solder. After they were cooled to room temperature, the specimens were machined. This machining included the removal of a 750 μm thick layer of copper from the sides of the specimens, as well as the drilling of the loading pin holes. A depiction of the DCB specimen, before and after the machining process, can be seen in Figure 2.4.

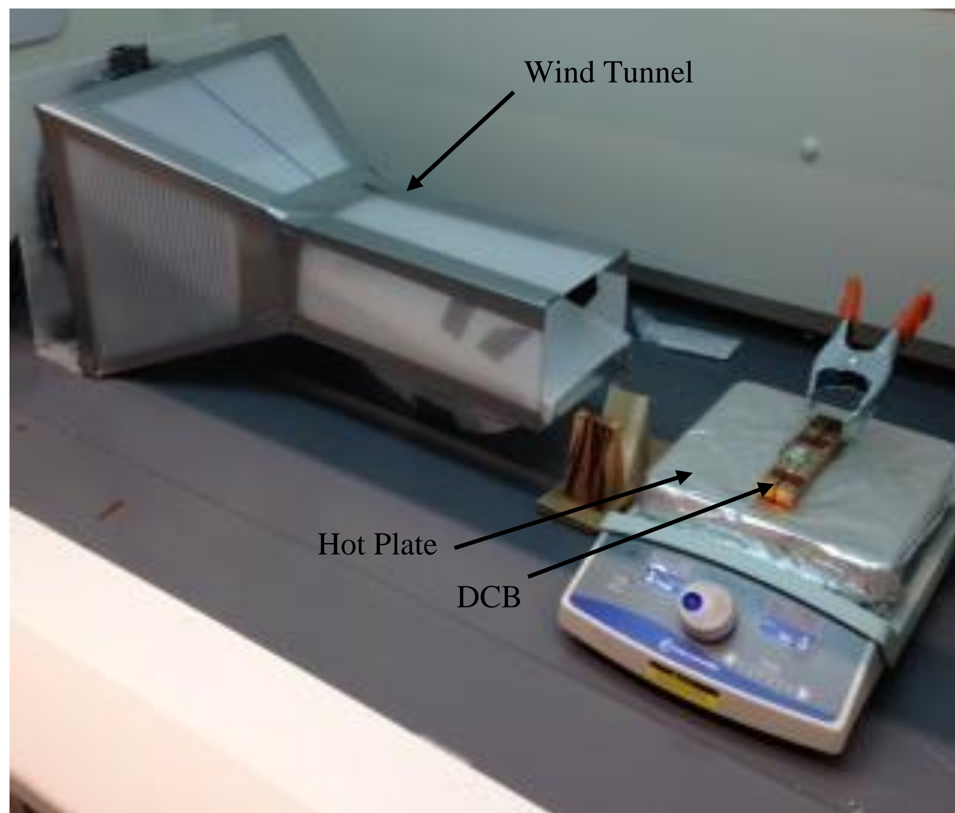

Figure 2.2 Image of sample preparation set-up.

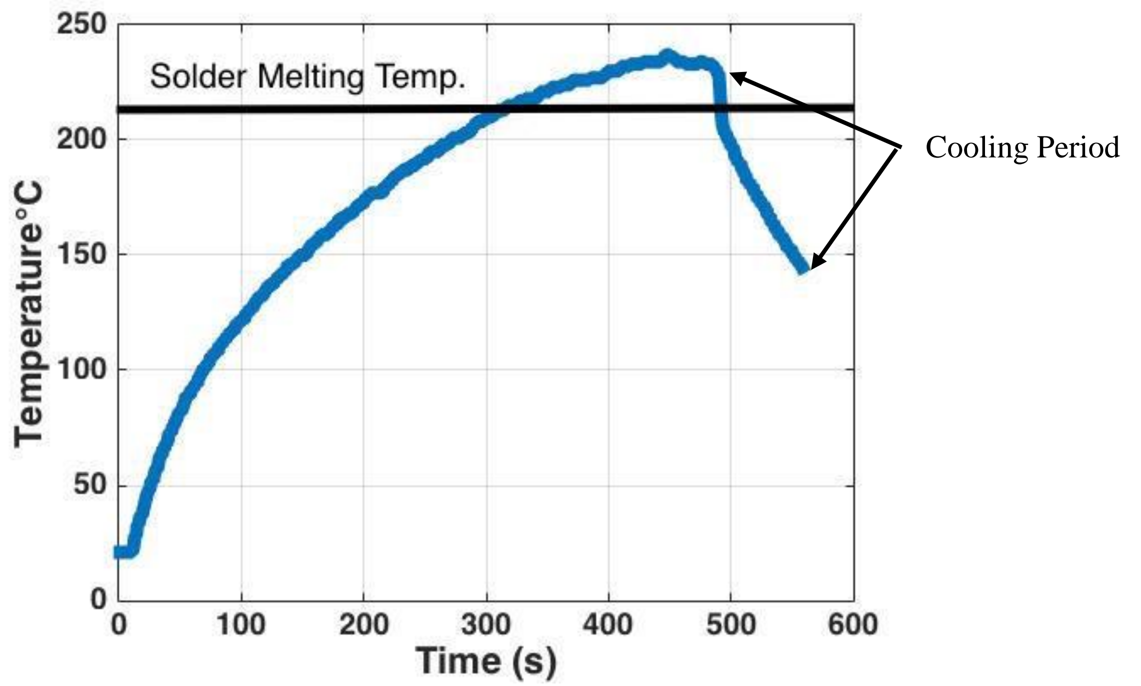

Figure 2.3 Time-temperature profile a DCB specimen during its fabrication**.**

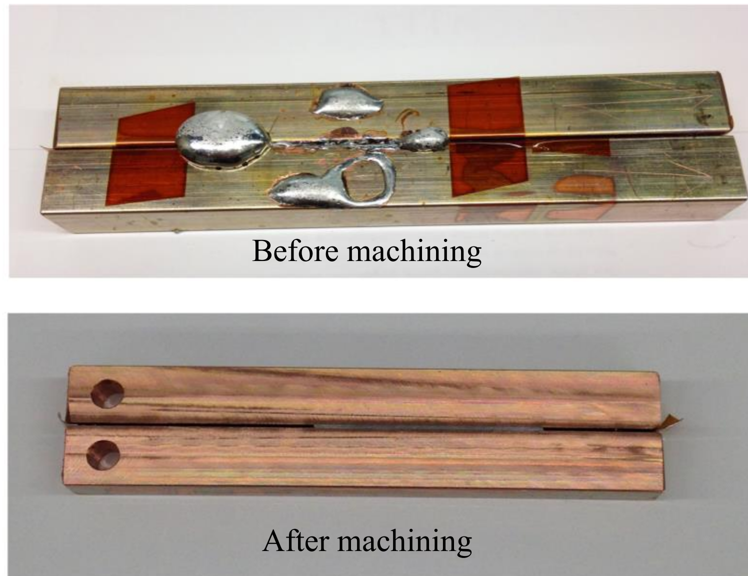

Figure 2.4 Before and after images of the DCB specimen.

2.2 Fracture Tests

The DCB specimens were fractured in mode-I under displacement control with a constant cross-head speed of 0.002 mm/sec at temperatures of 22°C and 100 °C. The crack initiation, defined by the appearance of a 100μm crack, and propagation were observed using an Edmund Optics monochrome USB 3.0 camera, with 2.0 MegaPixel resolution. The camera was paired with a Tamron telephoto 180 mm macro lens, which could provide 1:1 magnification. This methodology was followed in all the experiments reported here. Table 2.1 shows the number of DCB specimens tested at each temperature. All of the experiments were conducted inside of a Thermcraft oven. Figure 2.5(a) depicts the entire experimental setup, including the load frame, environment chamber and camera/ lens. The specimen loading scheme can be seen, in greater detail, in Figure 2.5(b). The force associated with crack initiation was identified by visual inspection.

Table 2.1 Number of Specimens Tested at each Temperature

Temperature (°C)	Number of Samples Tested
22	8
100	3

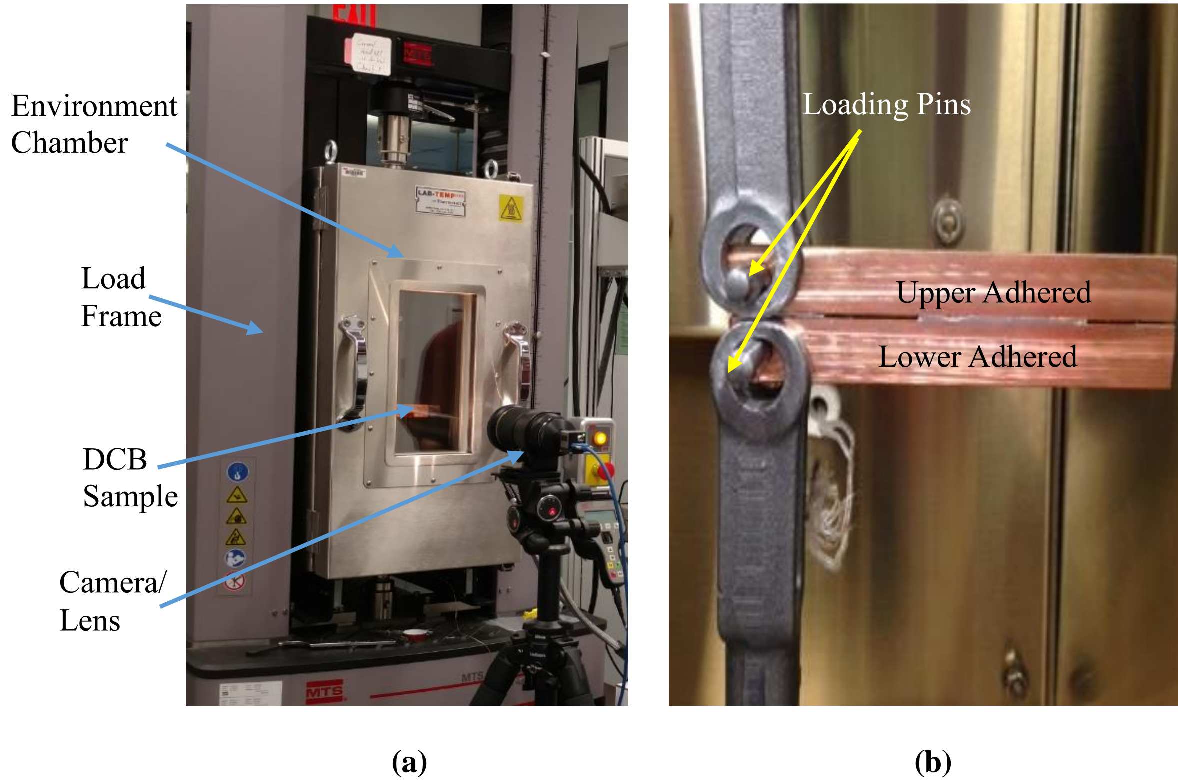

Figure 2.5 Image of **(a)** experimental set-up. **(b)** DCB inside the environmental chamber.

CHAPTER 3

J-INTEGRAL AND FINITE ELEMENT MODELING

3.1 The J-Integral

The J-integral proposed by Rice [19] is the appropriate fracture parameter for this study of the ductile lead-free solder. Mathematically, the J-integral is presented as a path integral in equation 3.1. Here, T_i and u_i are the applied traction and displacement vector respectively. The path of the J-Integral is represented by Γ and ds is an increment of this path. Lastly, W, x_1 and n_1 represent the strain energy density, coordinate axis and normal in the direction of crack growth, respectively. Since it is path independent, the aforementioned path of the integral can be chosen arbitrarily [17]. A physical interpretation of the J-Integral is provided in Figure 3.1; it represents the rate of change of the potential energy with respect to a unit crack extension; the shaded region in the figure.

$$J = \int_{\Gamma} \left[W n_1 - T_i \frac{\partial u_i}{\partial x_1} \right] ds \qquad (3.1)$$

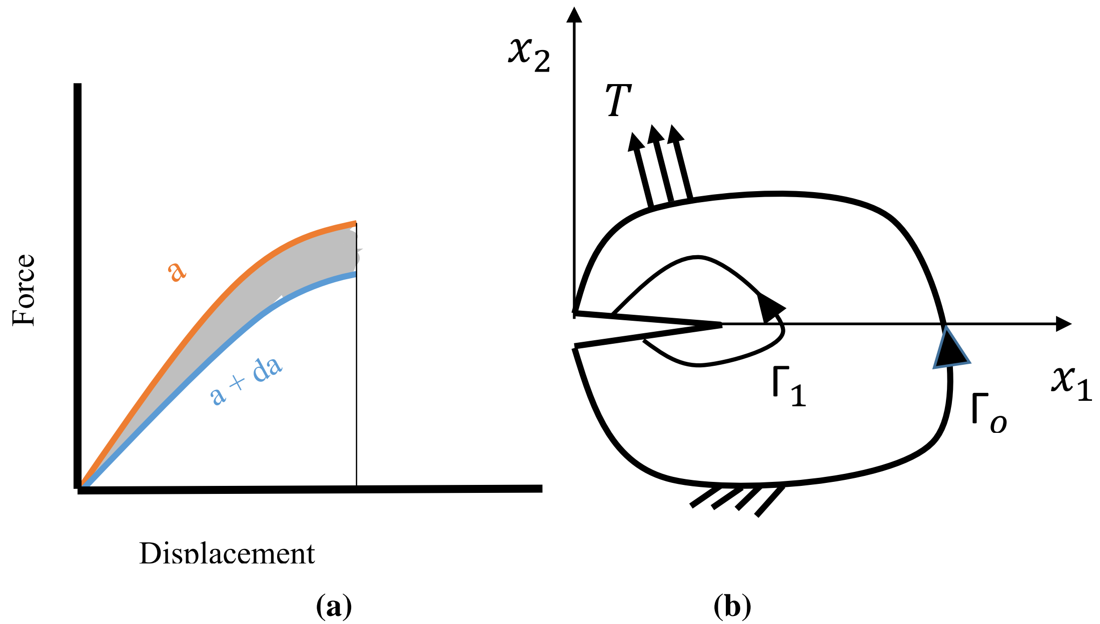

(a) **(b)**

Figure 3.1 (a) Schematic of the change in potential energy of a nonlinearly elastic material. The shaded region can be estimated from J-integral calculations. **(b)** Crack enclosed by contours [17].

3.2 Finite Element Calculation of J_c

Nadimpalli et al. [11, 18] have developed a finite element model of a DCB sample in a commercial finite element package ANSYS which, explicitly, models a crack in the middle of the solder layer; a similar methodology was adopted here, see Fig. 3.2. PLANE 183 elements were used to mesh the model. Since the solder layer was relatively thin and constrained by the copper bars, it was modeled in plane strain. The copper bars were unconstrained, with loads applied perpendicularly, therefore the copper was modeled in plane stress. Near the crack tip, the mesh consists of 6-node triangular elements which were formed by collapsing 8-node PLANE 183 elements. These singular elements were maintained at a length of 0.02 mm. In order to ensure the presence of 20 elements in the solder layer, the mesh was graded. The finite element mesh, along with boundary

conditions, is shown in Figure 3.2. Table 3.1 contains the material properties which were used in the finite element model. Assigning linear elastic isotropic and isotropic plastic material properties to copper and solder respectively, this model is used to compute the J-integral value corresponding to the failure loads obtained from the experiments. The path integral showed in equation 3.1 can be converted into an area integral as shown in equation 3.2 by using the divergence theorem.

$$J = \int_A \left[\sigma_{ij} \frac{\partial u_j}{\partial x_1} - w\delta_{1i}\right] \frac{\partial q}{\partial x_i} dA \qquad (3.2)$$

Where σ_{ij} and u_j are the stress tensor and displacement vector respectively. The Kronecker delta is represented by δ_{1i}. Additionally, q and w are the crack-extension vector and strain energy density respectively. The coordinate axis is represented by x_i. This area integral can be conveniently evaluated using finite element models. In order to compute the J-integral, the model takes the specimen geometry, crack initiation force and material properties as inputs. Two additional critical inputs are: a node/ group of nodes at the crack tip and the direction of crack extension.

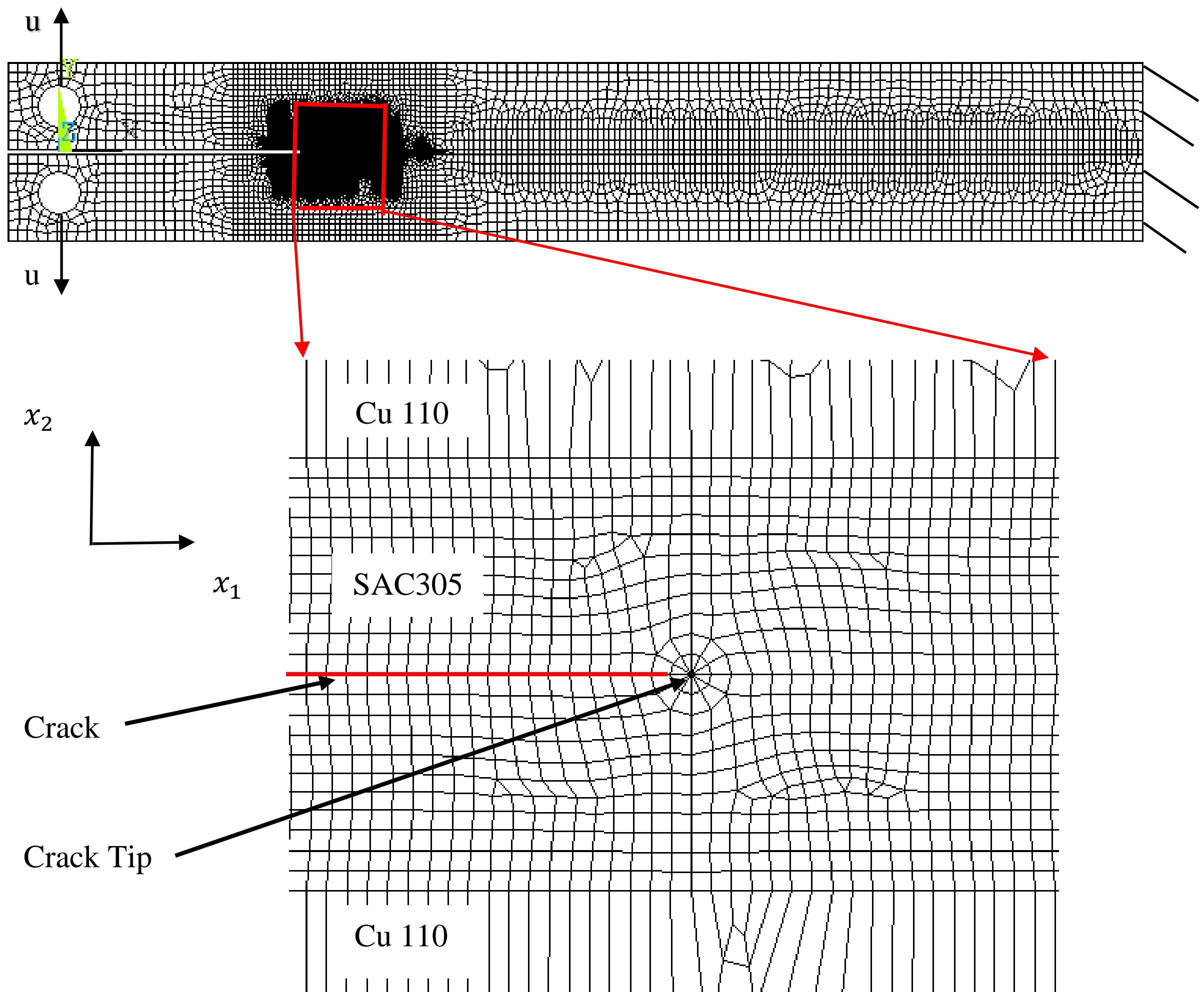

Figure 3.2 FE mesh of DCB with loads and boundary conditions.

Table 3.1 Mechanical Properties used in Finite Element Analysis

Temperature (°C)	Material	Young's Modulus (GPa)	Poisson Ratio
22	Copper	124	0.35
	Solder	51	0.40
100	Copper	124	0.35
	Solder	51	0.40

CHAPTER 4
RESULTS AND DISCUSSION

4.1 Crack Initiation and J_c

Figure 4.1 depicts the typical force-displacement response of a sample at 22 °C and 100 °C. The displacement referred to in this figure is that of the load frame's crosshead. The crack initiation forces, indicated by asterisks, were 702 N and 316 N for 22 °C and 100 °C, respectively. These crack initiation loads have been identified by visual inspection method; an appearance of a crack of approximately 100µm long is defined as crack initiation. The force increased linearly with crosshead displacement as the crack propagated after initiation. After extensive crack growth, the force response became nonlinear, reached peak, and gradually decreased for a short time followed by ultimate failure causing the sample to break into two pieces. This behavior was similar in all the samples tested in this study. Given the ductile nature of SAC305 solder, this type of extensive crack propagation behavior was expected.

It can be seen, from Figure 4.1 that the critical loads corresponding to crack initiation, indicated with a marker, as well as the peak loads associated with crack propagation decreased with an increase in the temperature, i.e., the initiation and propagation of crack becomes easier at high temperatures. The J-integral values corresponding to crack initiation loads were evaluated according to the methods explained in Chapter 3 and plotted in Figure 4.2. As expected, the fracture energy of the Cu/SAC305/Cu joints decreased with increase in temperature. A similar trend has been observed in other metals by Kanel et al. [14], i.e., spall strength decreased as the

temperature approached the material's melting temperature [14-16]. The decrease in fracture energy can be attributed to the temperature dependent mechanical properties of solder and crack formation mechanisms.

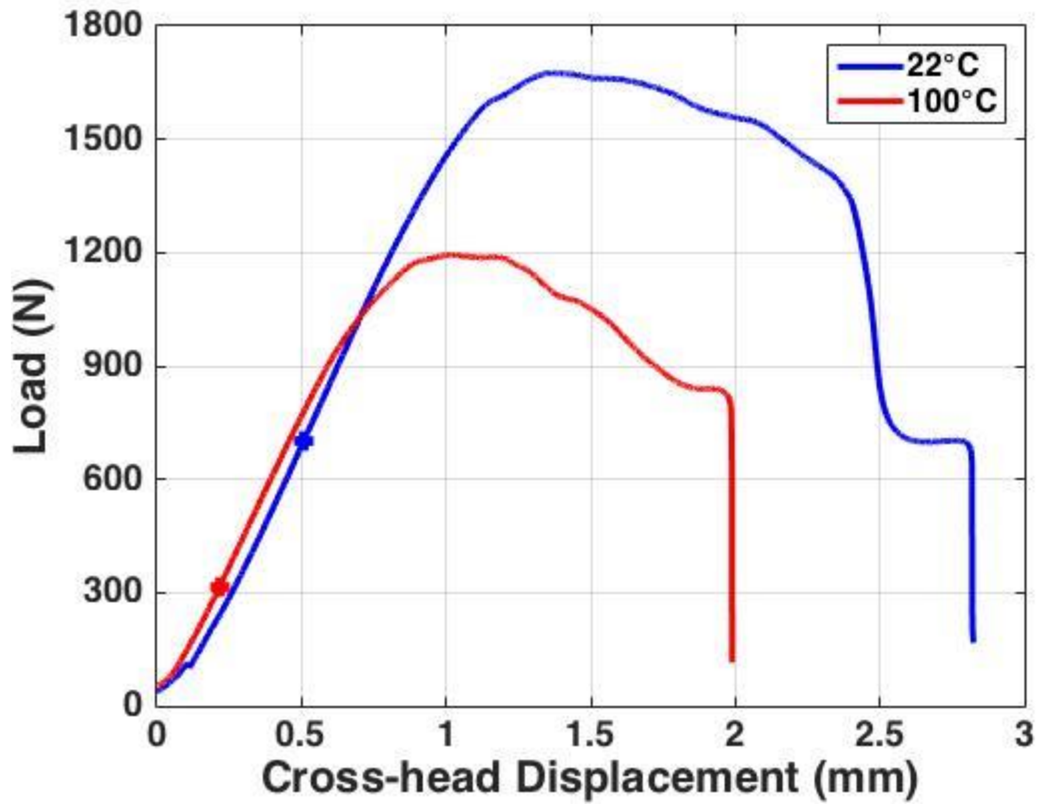

Figure 4.1 Load-displacement response of DCB sample.

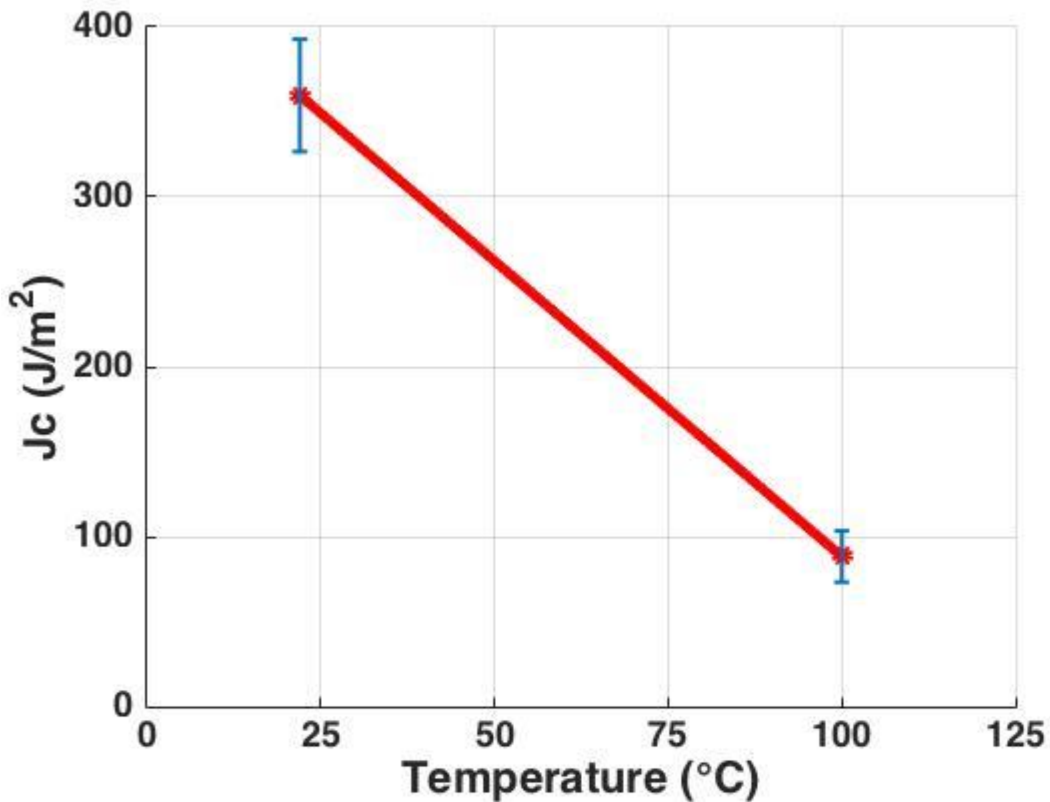

Figure 4.2 Fracture energy release rates.

4.2 Crack Path Analysis

To understand the reasons for the trend in fracture energy, the fracture surfaces of the samples were analyzed. Figures 4.3a and 4.3b show the fracture surfaces of samples tested at 22 °C and 100 °C, respectively. It was observed that, although the crack propagated within the solder layer in both cases, the path was close to the interface for the 100 °C sample. These surfaces were further observed in SEM to identify the failure mechanisms and microstructural features which motivated the trend observed in Figure 4.2. Figure 4.4a shows dimple type features which are a signature of ductile failure whereas Figure 4.4b shows brittle fracture surface with the crack path through the intermetallic region. These observations support the trend shown in Figure 4.2 as brittle

failure generally leads to a smaller fracture energy. Although these SEM images confirm the observations of Figure 4.3 and trends in Figure 4.2, the SEM analysis was conducted on very few samples. Also, it is not yet known why an increase in temperature would cause a brittle failure through the intermetallic region, near the interface. Hence, a more thorough investigation is necessary to identify the mechanisms of failure and explain the trend in Figure 4.2.

It should be noted that, although the microstructural analysis and fracture surface analysis were not complete and thorough, the fracture energy data as a function of temperature, presented in Fig. 4.2, will be valuable to microelectronic packaging engineers. At present, the package designers do not have access to such data. This lack of information will lead to packaging designs which may not be optimized for higher reliability.

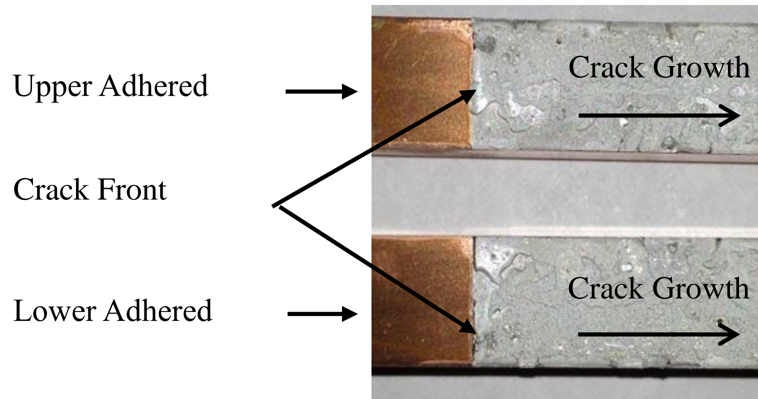

(a)

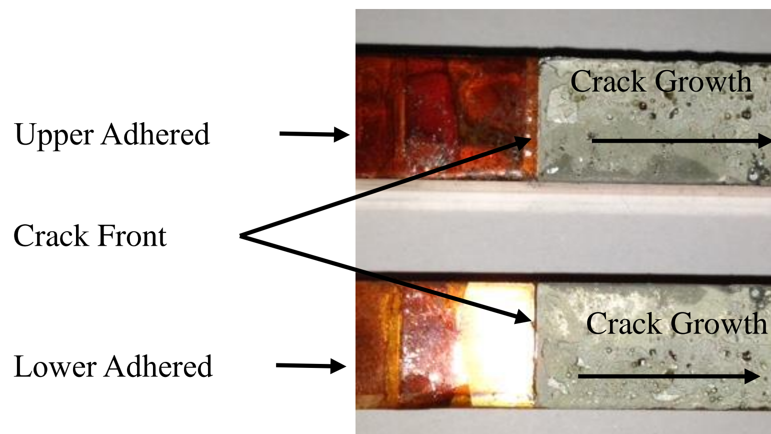

(b)

Figure 4.3 Fracture surface of DCB tested at (a) 22 ºC. (b) 100 ºC.

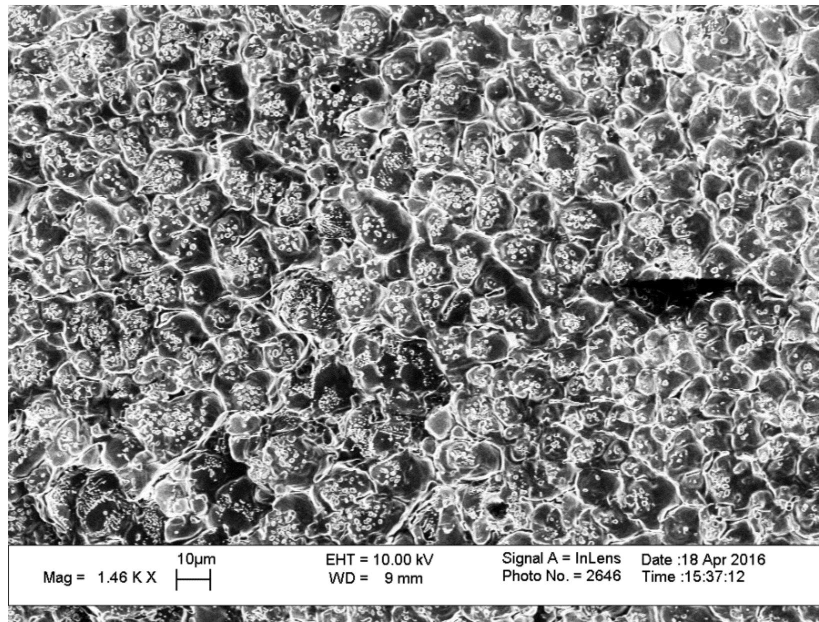

(a)

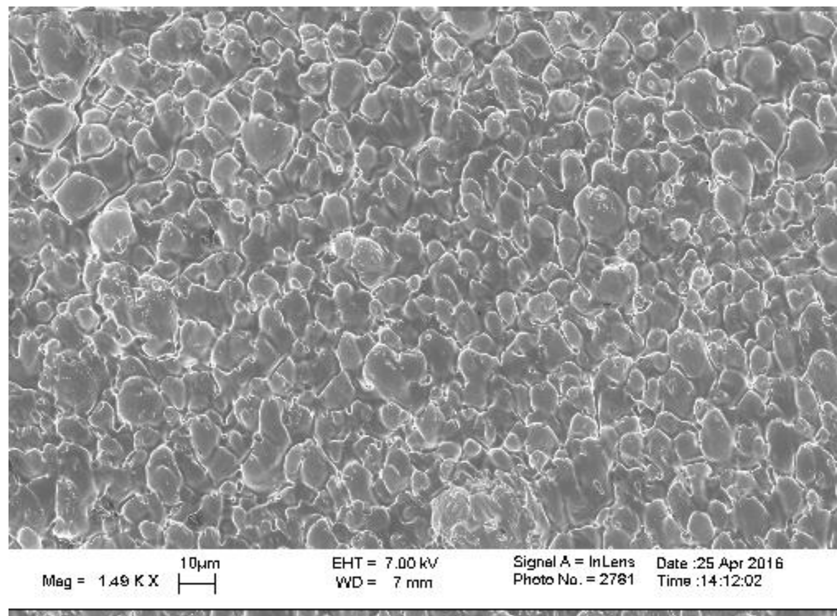

(b)

Figure 4.4 SEM Images of samples tested at **(a)** 22 ºC. **(b)** 100 ºC.

CHAPTER 5
CONCLUSIONS

5.1 Summary of Findings

A continuous layer of SAC305 solder was sandwiched between two copper bars and prepared under standard surface mount (SMT) processing conditions. Then the specimens were fractured under mode-I loading at various temperatures. The load corresponding to crack initiation was recorded and used to compute the critical fracture energy (J-integral) corresponding to crack initiation.

It was determined that the toughest specimens were those tested at room temperature. The specimens exhibited characteristics of ductile fracture at room temperature. Conversely, those tested at 100 ºC exhibited characteristics of brittle fracture. Based on past studies [14-16], the observed relationship between temperature and fracture toughness was expected. These results will provide valuable information to manufacturers of microelectronics packages, as well as consumers.

5.2 Future Work

The present study has thoroughly examined the effect of elevated temperatures on the fracture properties of SAC305 solder. However, these properties have only been measured under Mode-I loading. It could be expanded upon by studying the effects of mixed-mode loading at various temperatures. Another promising study could be one of the effects of strain rate, at various temperatures, on the fracture properties of SAC305 solder.

REFERENCES

[1] Kim, J.W., Jung, S.B. "Experiment and finite element analysis of the shear speed effects on the Sn-Ag-Cu BGA solder joints." Mater. Sci. Eng. A 371 (2004): 267-276.

[2] JESD 22-B117A, JEDEC Solid State Technology Association, Arlington, VA, USA, 2006.

[3] Newman, K. "BGA brittle fracture – alternative solder joint integrity test methods." In: Electron compon tech conf; (2005): 1194-201.

[4] Seah, S.K.W, Wong, E.H., Mai, Y.W., Rajoo, R., Lim, C.T. "High-speed bend test method and failure prediction for drop impact reliability," In: Electron compon tech conf; (2006): 1003-08.

[5] Chong, D.Y.R., Che, F.X., Pang, J.H.L., Ng, K., Tan, J.Y.N., Low, T.H. "Drop impact reliability testing for lead-free and lead based solder IC packages," Microelectronics Reliability 46 (2006):1160-71.

[6] JESD 22-B111, JEDEC Solid State Technology Association, Arlington, VA, USA, 2003.

[7] Tan, L.B., Xiaowu, Z., Lim, C.T., Tan, V.B.C. "Mapping the failure envelope of board-level solder joints," Microelectronics Reliability 49 (2009):397-409.

[8] Fernlund, G., Spelt, J.K. "Failure load prediction of structural adhesive joints," Part 1: analytical method. Int J Adhes 11 (1991):213-20.

[9] Fernlund, G., Spelt, J.K. "Mixed mode energy release rates for adhesively bonded beam specimens," J Compos Technol Res 16 (1994):234-43.

[10] Azari, S., Eskandarian, M., Papini, M., Schroeder, J.A., Spelt, J.K. "Fracture load prediction and measurements for highly toughened epoxy adhesive joints," Engineering Fracture Mechanics 76 (2009): 2039-55.

[11] Nadimpalli, S.P., Spelt, J.K. "Fracture Load Prediction of Lead-free Solder Joints." Engineering Fracture Mechanics 77 (2010): 3446-3461.

[12] Huang, Z. "Fracture of Lead-Free Solder Joints for Electronic Applications: Effect of Material, Processing and Loading Conditions." *Wsulibs*. https://research.wsulibs.wsu.edu/xmlui/bitstream/handle/2376/4709/Huang_wsu_0251E_10629.pdf?sequence=1.

[13] Dieter, G.E. *Mechanical Metallurgy* (London: McGraw-Hill, 1988), 241, 432.

[14] Kanel, G.I., Razorenov, S.V., Bogatch, A. "Spall Fracture Properties of Aluminum at High Temperatures." J. Appl. Phys 79 (1996): 8310.

[15] Zhu, M.L., Xuan, F.Z. "Effect of Temperature on Tensile and Impact Behavior of Dissimilar Welds of Rotor Steel." Materials & Design 31 (2010): 3346-3352.

[16] Logsdon, W.A., Liaw, P.K., Burke, M.A. "Fracture Behavior of 63Sn-37Pb Solder." Engineering Fracture Mechanics 36 (1990): 183-218.

[17] M.F. Kanninen and C.H. Popelar. *Advanced Fracture Mechanics* (New York: Oxford University Press, 1985),138-188, 281.

[18] Nadimpalli, S.P., Spelt, J.K. "Mixed-mode Fracture Load Prediction in Lead-free Solder Joints." Engineering Fracture Mechanics 78 (2011): 317-333.

[19] Rice, J.R. "A Path Independent Integral and the Approximate Analysis of Strain Concentration by Notches and Cracks." Journal of Applied Mechanics 35 (1968): 379-386.